MJFAS
Malaysian Journal of Fundamental and Applied Sciences

John *et al.* | Malaysian Journal of Fundamental and Applied Sciences, Vol. 19 (2023) 936-946

RESEARCH ARTICLE

Improved Performance of Optical Fiber Core: Role of Plasmonic Metals Activation

Hussein Taqi John[a], Oday Jawad Kadhim[a], Imad Kamil Zayer[a], M S Aziz[b], A A Salim[b*]

[a]Physics Department, College of Science, Wasit University, Wasit, Iraq; [b]Laser Centre & Physics Department, Faculty of Science, Universiti Teknologi Malaysia, 81310 UTM Johor Bahru, Johor, Malaysia

Abstract Optical fiber core with customized characteristics became demanding for diverse high performance applications. Based on this idea, the optical fiber core was activated using various plasmonic metals (beryllium, chromium, and nickel) to improve its refractive index, sensitivity and bandwidth. The influence of various wavelengths and core radii on three modes (LP_{01}, LP_{11} and LP_{21}) propagation was determined using finite element analysis (FEM). The COMSOL MULTIPHYSICS software was used for the computation. The fiber core radii of the plasmonic metal activated and wavelengths were varied to control the forward and backward energy propagation as well as the modal dispersion relation. Quantities like effective refractive index, attenuation, propagation constant and diffusion coefficient for the three modes as a function of wavelengths and fiber core radii were calculated, which showed maximum values at shorter wavelengths. Irrespective of the type of metal activation in the fiber core, the refractive index of LP_{01} mode for the core of radius 200 nm was more significantly affected compared to others. Regardless of different metals inclusion, the dispersion relation (refractive index versus frequency) for all modes was strongly positive, showing increasing values for radius in the order of 200, 400, 600 nm. Plasmonic metals Cr and Ni displayed best effect, while Be required high values of V to get LP_{01} in a narrow range and other modes appeared in a larger range than V. Present results may be useful for the development of high performance optical fiber core.

Keywords: Attenuation coefficient, plasmonic metals, propagation constant, refractive index, dispersion relation, modes.

Introduction

A plasmon is the quanta of plasma (electrons and ions density) oscillation [1,2] which is considered as a quasiparticle like phonons (quanta of lattice vibrations) [3]. Briefly, the plasmons are mass oscillations of the free electron gas density, especially prominent in the noble metal nanostructures due to strong localization (called quantum confinement) [4]. At optical frequencies these plasmons can couple with a photon to form another quasiparticle called plasmon polariton which can be described Maxwell's electromagnetic equations [5,6]. These plasmons play a significant role in the improvement of semiconductors and metals optical properties [7]. In the case of metals, the plasma frequency lies in ultraviolet region, making them reflective in the visible region. Various metals like copper, silver, and gold display visible interfacial electronic transitions, imparting their distinctive color upon absorbing certain wavelengths [6]. For semiconductors, the plasmon frequency of electrons oscillation occurs in the deep UV region, while the electronic its transitions across the bands occur in the visible region, producing characteristic colors and become reflective when certain light energies get absorbed [8-10].

Surface plasmon polariton (SPP) is the electromagnetic surface wave that propagates in a direction parallel to the interface of insulating materials. Since the propagated waves lie on the boundary of a conductor and an external medium like air, thereby very sensitive to any change in the boundaries. This in turn, alters the refractive index at the contact region, enabling the modulation of the surface plasmon resonance (SPR)-mediated strong electromagnetic field [11]. This unique feature allows the monitoring of the surface events that cause dielectric changes in the optical fiber desired for plasmonic applications [11].

***For correspondence:**
asali@utm.my

Received: 14 May 2023
Accepted: 21 Sept. 2023

Considering the immense importance of the highperformance optical fiber, we incorporate three plasmonic metals, mainly beryllium (Be), chromium (Cr), and nickel (Ni), into the fibre optic core in order to enhance the refractive index, attenuation coefficient, propagation constant, and dispersion relation for LP01, LP11, and LP21 modes. This allows us to compare their performance with the most effective metal and determine the optimal choice. Plasmonic metals are comprised of metallic constituents that demonstrate significant resistance to oxidation, even when exposed to elevated temperature conditions and chemical reactions [12]. This characteristic renders them highly resistant to corrosion and less susceptible to damage from acid attacks. In addition, photonic metals including gold (Au), silver (Ag), copper (Cu), aluminium (Al), platinum (Pt), Ni, Be, and Cr are renowned for their excellent conductivity and catalytic characteristics. These properties allow them to efficiently expedite or stabilize the kinetics of specific oxidation, reduction, and hydrogenation reactions [13]. Although these metals with outstanding localized surface plasmon resonance (LSPR) and resistance are still exposed to oxidation, leading to formation of metal oxides that are rather stable nature. Furthermore, these elements are among the best for forming the plasmonic phenomena due to their high absorption potential, ability to produce surface waves and other properties [12-14]. The effects of varying wavelengths and core radii on the propagation characteristics of these modes were evaluated using COMSOL MULTIPHYSICS software calculation. The plasmonic metals activation in the optical fiber core was shown to be useful for the customization of the propagation energy and dispersion relation. The computed results were analyzed, interpreted and discussed to gain a basic insight of the plasmonic effects on the optical fiber core properties.

The current work discusses the production of the plasmonic phenomena by creating the optical fibre cores from noble metals or plasmonic metals. It is evident that an optical fibre comprising a glass core lacks the capability to exhibit a plasmonic phenomenon, as this particular phenomenon exclusively occurs between two metallic media [15]. Numerous scholars have conducted investigations and implemented this phenomenon. Guo *et al*. [16] developed Plasmonic immunosensors using noble metal materials in the form of films or nanoparticles, which were functionalized with bioreceptors, enabling the detection of analytes through antibody/antigen interactions or other affinity-based mechanisms. The surface plasmon resonance (SPR) is excited by a localized discharge focused light. Today, photo-printed metal-coated fibre gratings within the fibre core are being considered for their modular features that enable SPR generation at any desired wavelength with a specific focus on communication window [17]. Scientists and researchers have achieved significant advancements in this particular sector by using several forms of gratings, including short inclined, uncentred, uniform, and long-term gratings [18]. The implementation of such sensors has been shown to be feasible for highly precise analysis and diagnostic applications conducted within living organisms [19]. Salman *et al*. [20] designed a sensor based on photonic crystal fibre (PCF) with an inner gold layer, positioned between the liquid holes and air holes between liquid and air holes to induce plasmonic effect. It was revealed that the thickness of the gold layer, the radius of the air and liquid holes exert a notable influence on the sensor's sensitivity, specifically under specific simulated conditions. Furthermore, the resonance wavelength was linearly related to the liquid's refractive index, allowing the analysis to be scaled without necessitating modifications to the sensor design [21]. Hussein *et al*. [22] constructed a plasmonic optical fibre sensor for sensing liquid materials using the imaginary component of the effective refractive index, which is responsible for the attenuation of these materials. The proposed sensor comprises two sets of circuits: the initial set consists six holes filled with air, while the external set is filled in an alternating mode with analytics and air. This configuration is then coated with a nickel and enclosed by a perfectly match layer (PML) to activate SPR and reduces reflections within the sensor's core, hence enhancing the sensor efficiency. The Druid-Lorentz model was used to compute metal electrical permittivity, while the Silimer model was utilised for silica [23].

Optical Fiber Design

The proposed fiber was composed of two concentric circles wherein the inner one of radius a represented the core (individually made from Cr, Ni, and Be) and the outer ring made from silica of radius b was the fiber clad (Figure 1a). Table 1 shows the values of fiber parameters. A series of distinct mathematical equations were used to split the fiber cross-section into infinitesimal called mesh as displayed in Figure 1b. The optical properties of the proposed plasmonic optical fiber material were determined using the FEM method in the COMSOL MULTIPHYSICS 5.4 environment. This software is based on the numerical simulation method, containing several physical models that allow in designing various engineering structures using computer-aided drawing (CAD). The FEM was used to solve the differential equations depending on fiber core mesh size. The behavior of the core medium was simulated via the summation of the differential equations for various meshes.

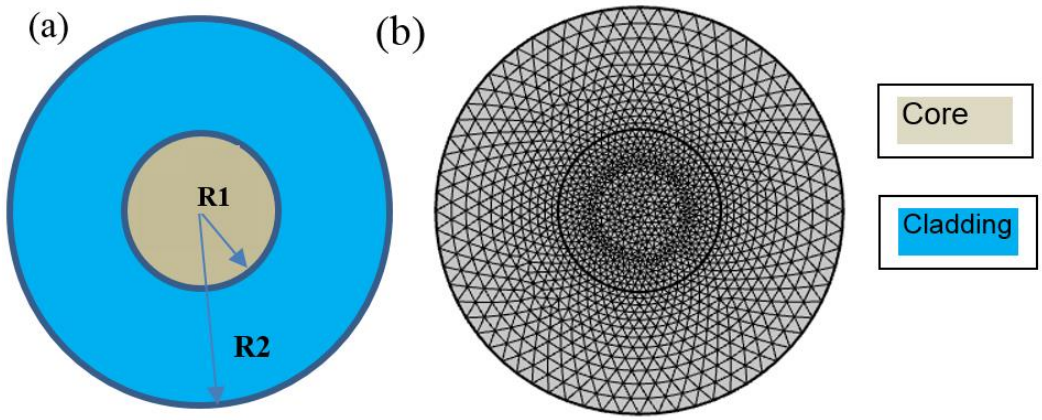

Figure 1. (a) Cross section and (b) mesh of the proposed fiber

Table 1 exemplifies the parameters and corresponding values utilized in the design of the plasmonic optical fibre, such as the wavelengths of incident light (ʎ), core and cladding radii (R1 and R2), clad refractive index (n_{clad}), core and cladding materials, which are determined via the COMSEL programme. It is important to emphasise that the selection of distinct radii for the core and envelope of the plasmonic optical fibre was based on experimental investigations and a comprehensive review of relevant literature sources [15, 24]. In particular, it was revealed that optimal plasmonic phenomenon outcomes were obtained when the core radius varied from 200 to 600 nm and the casing radius remained fixed at 1000 nm.

Table 1. Various parameters and their values of the optical fiber

Parameters	Values
Wavelength (ʎ)	1200 to 2000 nm with step size 100
Core radius (R1)	200, 400 and 600 nm
Clad radius (R2)	1000 nm
Clad refractive index (n_{clad})	1.45
Core	Be, Cr, Ni
Cladding	Silica

Theoretical Formalism

It is known that the fluctuating conduction electrons undergo inter-band transition when the incoming photon energy is higher than the band gap energy of the material. The transition probability is determined by the permittivity and permeability (complex dielectric functions) of the material. The optical properties of the material are affected by both bound and free electrons. The complex permittivity of the noble metals can be described by the Drude and Lorentz models given by [25]:

$$\varepsilon_r(w) = 1 - \frac{w_p^2}{w^2 + i\bar{\gamma}w} + \sum_i \frac{f_i w_i^2}{w_i^2 - w^2 - i\bar{\gamma}_i w} \qquad (1)$$

where w_i, i, $\bar{\gamma}_i$, and f_i are the resonance frequencies, resonating patterns, damping coefficient and weighted factors of the metals. Table 2 presents the various parameter values of the Drude-Lorentz model used in this work for different metals.

Table 2. Parameter values of different metals used in equation 1 [26]

Parameters	Be	Cr	Ni
f_o	0.084	0.168	0.096
γ_d	0.035	0.047	0.048
f_1	0.031	0.151	0.100
γ_1 (eV)	1.664	3.175	4.511
w_1 (eV)	0.100	0.121	0.174
f_2	0.140	0.150	0.135
γ_2	3.395	1.305	1.334
w_2	1.032	0.543	0.582
f_3	0.530	1.149	0.106
γ_3	4.454	2.676	2.178
w_3	3.183	1.970	1.597
f_4	0.130	0.825	0.729
γ_4	1.802	1.335	6.292
w_4	4.604	8.775	6.089
f_5	—	—	—
τ_5	—	—	—
w_5	—	—	—

Since only the LP01 mode propagates in a single mode optical fiber, no time difference across the modes exist, resulting in the complete absence of multimodal dispersion. Also, each propagation mode is associated with the fiber core that satisfies the following condition [25]:

$$n_{clad} < n_{eff} < n_{core} \quad (2)$$

where $n_{eff} = \beta/k_0$ is the effective refractive index of the fiber core, β is the propagation constant, and $k0=2\pi/\lambda$ is the wave vector in vacuum with wavelength λ.
The attenuation coefficient (a measure of electromagnetic energy loss in the optical fiber) can be calculated using the expression [26]:

$$\alpha \approx 8.686 k_o im\{n_{eff}\} \times 10^7 \quad (dB/cm) \quad (3)$$

where im{n_{eff} } is the imaginary part of the effective refractive index.

The normalized frequency (V) can be used to determine the single-mode nature of the fiber at a given wavelength. In addition, it measured the number of possible associated modes given by [27]:

$$V = \frac{2\pi a}{\lambda}\sqrt{n_1^2 - n_2^2} \quad (4)$$

where a is core radius of the fiber.

Results and Discussion

The refractive index of the optical fibre core was determined using the equation $n = (\varepsilon\ \mu)^{1/2}$, assuming that all materials involved were non-magnetic materials. Hence, it may be inferred that the value of μ is equal to 1. This conclusion is based on the chemical classification of nickel as a transition metal, its weak magnetic properties, and its similarity in behaviour to noble metals [28]. The electrical permittivity was obtained using equation (1). The values of fiber parameters (Table 2) were used to calculate the modes by the COMSOL software. Figures 2 and 3 show the computed three modes including LP_{01} and LP_{11} and LP_{21}. The results were obtained for various fiber core radii (200, 400, and 600 *nm*) and various wavelengths (1000, 1500, and 2000 nm). For the fiber core made of Cr (Figure 2), the outgoing energy percentage from the core was increased with the increase of wavelength (indicated by the yellow and red color). For the core made of Ni (Figure 3), the mode size was increased with the increase of core radius. All three modes revealed similar trends. It was affirmed that the power ratio in the proposed may be controlled by adjusting the fiber core radius and wavelength. It has been observed that the simulation results (Figure 2 and 3) deviate from the well-established Gaussian intensity profile for the LP01 mode. This deviation can be attributed to the metallic composition of the plasmonic fiber's core, which causes the Gaussian density to be inadequate, only the ends remain. Additionally, the Gaussian intensity is only

observed in the insulating regions [29].

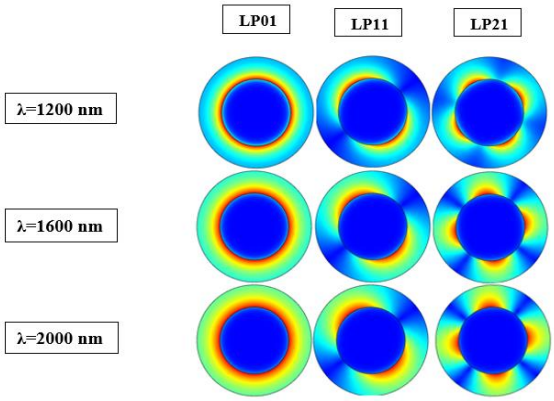

Figure 2. The modal features for Cr core fiber at a = 600 nm and λ=1200, 1600, and 2000 nm

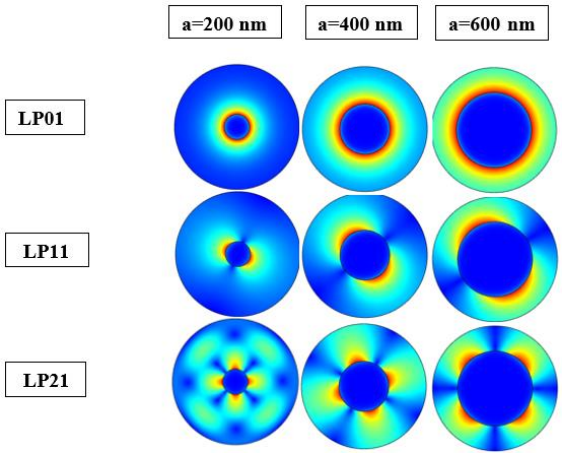

Figure 3. The modal features for Ni core fiber at λ = 1600 nm and a = 200, 400, and 600 nm

Figures 4 to 6 illustrate the relationship between n_{eff} and λ for LP_{01}, LP_{11}, LP_{21} modes propagation in the fiber cores made from Be, Cr, and Ni at various radii (200, 400, and 600 nm). Irrespective of the core types, the values of n_{eff} was highest at shortest wavelengths. With the increase of wavelength the values of n_{eff} for all modes were decreased. This observation can be attributed to the influence of SPR-mediated electromagnetic fields on the fiber core refractive index. The refractive index consisted of real and imaginary parts (the imaginary and real part signified the corresponding attenuation and refraction of light in the fiber material). Essentially, the refractive index was strongly affected by the plasmon waves and density of the fiber material. The change of n_{eff} with λ and *a* depending on the intensity of each mode was clearly evidenced. For the first time we designed this type of fiber with plasmonic metal core and demonstrated the strong correlation between n_{eff} and λ for LP_{01}, LP_{11}, LP_{21} modes at different core radii [30]. For LP_{01} mode (Figure 4), the values of n_{eff} were decreased with the increase of radii from 200 to 600 nm. Furthermore, the values of n_{eff} were identical for *a* = 400 and 600 nm for λ in the range of 1200 - 1300 nm. Then, the values started move away with the increase of wavelength (Figure 4b and c). The curves for *a* = 400, and 600 nm were coincided at the λ = 1400 nm and 1300 nm, respectively. Figures 5 and 6 corresponding to the LP_{11} and LP_{21} modes displayed highest value of n_{eff} at *a* = 600, 400, and 200 nm, respectively. A comparison of the results for 3 different plasmonic metal activated fiber core showed that the highest value of n_{eff} followed the trend of *Cr* > Ni > *Be*.

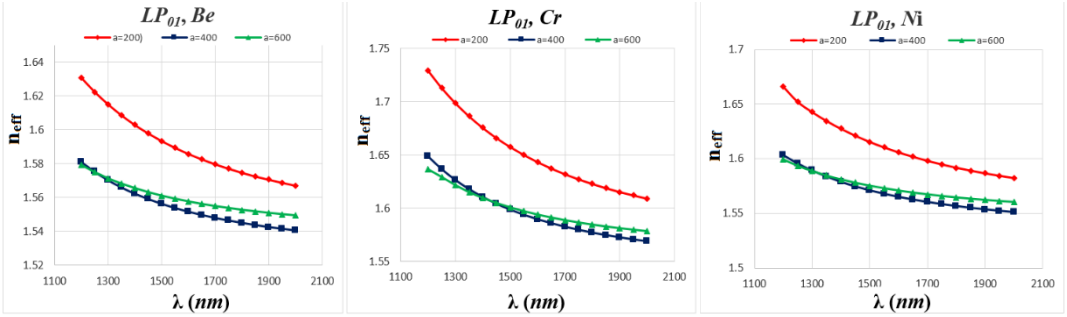

Figure 4. The neff versus λ for LP01 mode of the fiber cores made with Be, Cr and Ni at a = 200, 400, and 600 nm

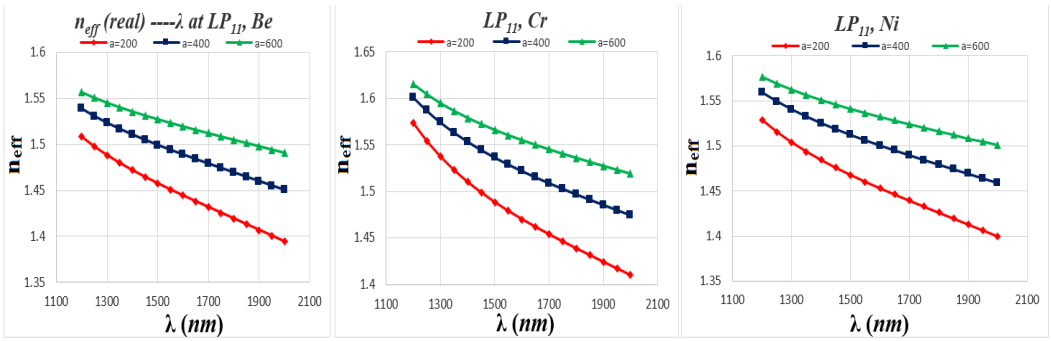

Figure 5. The n_{eff} versus λ for LP_{11} mode of the fiber cores made with *Be, Cr* and *Ni* at *a* = 200, 400, and 600 nm

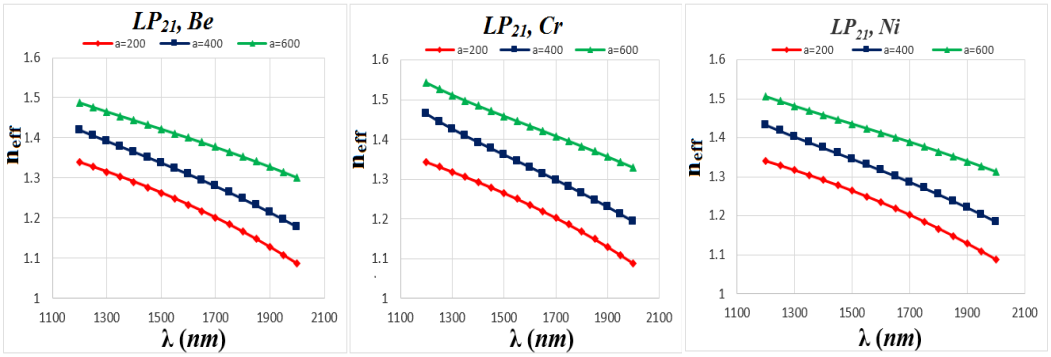

Figure 6. The n_{eff} versus λ for LP_{21} mode of the fiber cores made with *Be, Cr* and *Ni* at *a* = 200, 400, and 600 nm

Figures 7 to 9 present the attenuation coefficient (α) against λ relation for LP_{01}, LP_{11}, LP_{21} modes propagation in the fiber cores made from Be, Cr, and Ni at various radii (200, 400, and 600 nm). For all fiber cores, the values of α was maximum at shortest wavelengths and then decreased with the increase of λ, which was mainly due to the dependence of α (imaginary part of the effective refractive index) on the fiber core density (inversely proportional). For LP_{01} mode (Figure 7), the highest value α was obtained at *a* = 200. The value α at *a* =400 and 600 *nm* were further away from the one obtained at *a* = 200 *nm* except the point of co-occurrence at highest wavelength. For the fiber core made using Be, Cr and Ni it matched correspondingly at λ of 1600, 1690 and 1700 *nm*. For the mode LP_{11} (Figure 8) the value of α for different radii followed the trend of 600 > 400 > 200 *nm.* However, but these curves are identical from the beginning and then diverge with each other with increasing wavelength. For the core made using Be, all three curves were coincided at λ=1200 *nm.* For the core made from *Cr* and *Ni,* all three curves were correspondingly merged at λ=1400 *nm* and λ=1300 *nm*. For LP_{21} mode (Figure 9), the highest value of α for different radii followed the trend 600 > 400 > 200 *nm*. In addition, the curves for *a* = 400 and 600 *nm* were merged at far-off from *a* = 200 *nm*. A comparison of these results showed that the values of α followed the trend of *Cr* > *Ni* > *Be*. The value of α was used to characterize the penetration of a light

beam through the medium. Thus, the larger value of α signified a weaker penetration of the light beam through the medium thereby indicating high attenuation. In a concise manner. The graphs produced from the experimental analysis reveal that plasmonic optical fibers exhibit significant attenuation. The findings indicate that amongst the elements assessed, Cr exhibits the highest level of attenuation, followed by Ni and Be.

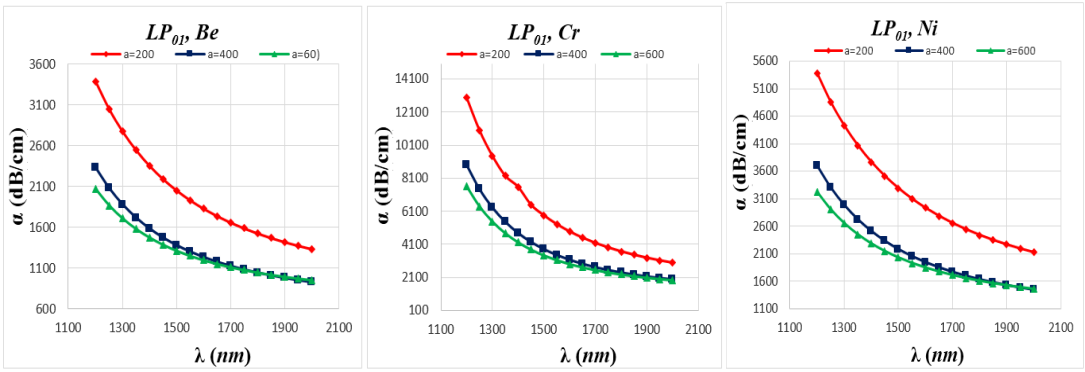

Figure 7. The α-λ relation for LP_{01} mode of the fiber cores made with *Be, Cr* and *Ni* at *a* = 200, 400, and 600 nm

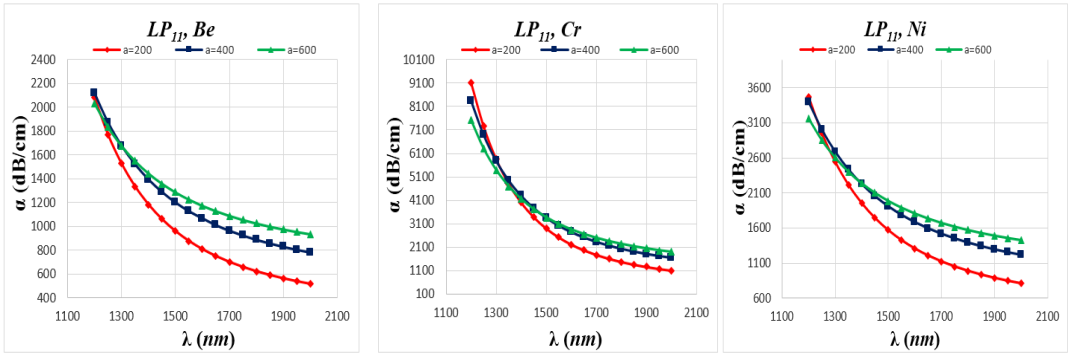

Figure 8. The α versus λ plot for LP_{11} mode of the fiber cores made with *Be, Cr* and *Ni* at *a* = 200, 400, and 600 nm

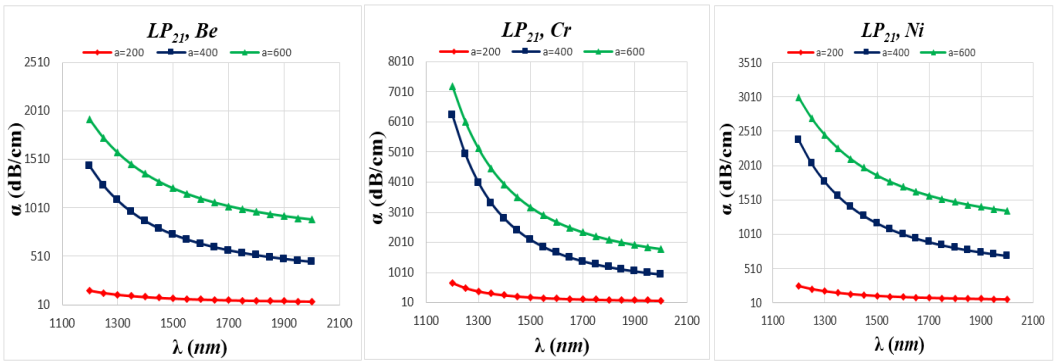

Figure 9. The α versus λ plot for LP_{21} mode of the fiber cores made with *Be, Cr* and *Ni* at *a* = 200, 400, and 600 nm

Figures 10 to 12 display the β against λ plot for LP_{01}, LP_{11}, LP_{21} modes propagation in the fiber cores made from Be, Cr, and Ni at various radii (200, 400, and 600 nm). For all fiber cores and regardless of the radii, the values of β was maximum at shortest wavelengths and then decreased with the increase of λ. This result can be ascribed to inverse dependence of β (diffusion or propagation constant) on the

real part of the refractive index and density of the medium. Thus, with the increase of the refractive index, the diffusion constant was decreased. For LP_{01} mode, the value of β was highest at *a* = 200 *nm* and then became identical at *a* = 400, 600 *nm*. Finally, all these curves were merged at the highest wavelength. The values of β for the fiber core made from different metals followed the trend of *Cr* > *Ni* > *Be.* For LP_{11} and LP_{21} modes (Figures 11 and 12), the values of β for the fiber core of different radii followed the trend of 600 > 400 > 200 *nm*. Additionally, all the curves for 3 plasmonic metals were convergent, except for the mode LP_{11}. A comparison of the results for 3 different metal cores displayed that the value β attained the order of *Cr* > *Ni* > *Be*.

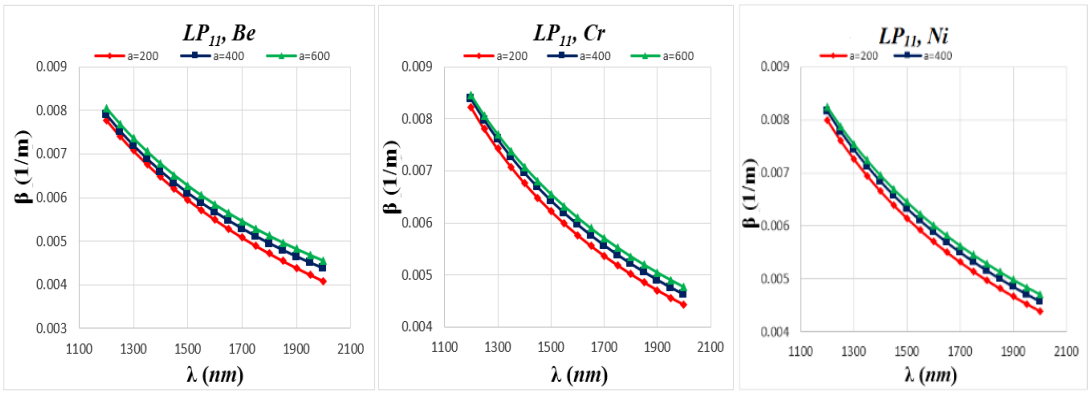

Figure 10. The β-λ relation for LP_{01} mode of the fiber cores made with *Be, Cr* and *Ni* at *a* = 200, 400, and 600 nm

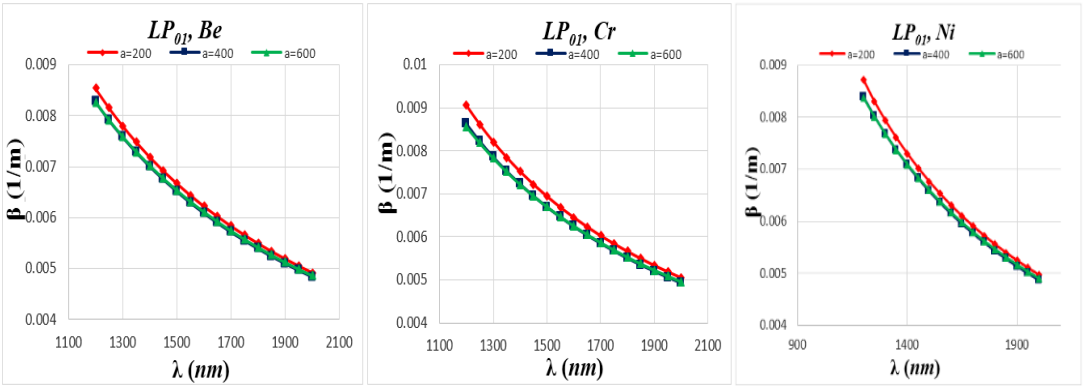

Figure 11. The β-λ relation for LP_{11} mode of the fiber cores made with *Be, Cr* and *Ni* at *a* = 200, 400, and 600 nm

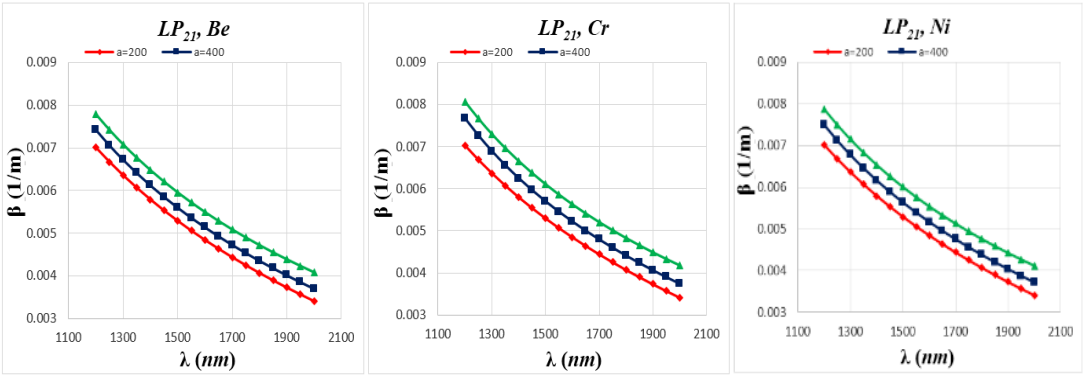

Figure 12. The β-λ relation for LP_{21} mode of the fiber cores made with *Be, Cr* and *Ni* at *a* = 200, 400, and 600 nm

Figures 13 to 15 show the dispersion relation (V versus n_{eff}) for LP_{01}, LP_{11}, LP_{21} modes propagation in the fiber cores made from Be, Cr, and Ni at various radii (200, 400, and 600 nm). For all fiber cores, the values of n_{eff} was maximum at the lowest normalized frequency (V) and then decreased with the increase of V. in addition, a direct relation between n_{eff} and V was discerned, wherein the value of V was increased with increase of n_{eff}. This improvement in the n_{eff} value as a function of the core radii followed a trend of 200 > 400 > 600 nm. The values of of n_{eff} for the core radius 499 and 600 nm were very close to each other and far away from the n_{eff} values obtained with core radii of 200 nm. For all modes, the fiber core made from Cr showed optimum values of V followed by Ni and Be. It was observed that the mode LP_{01} appeared in a narrow range of V and modes LP_{11}, LP_{21} occurred in a wider range of V.

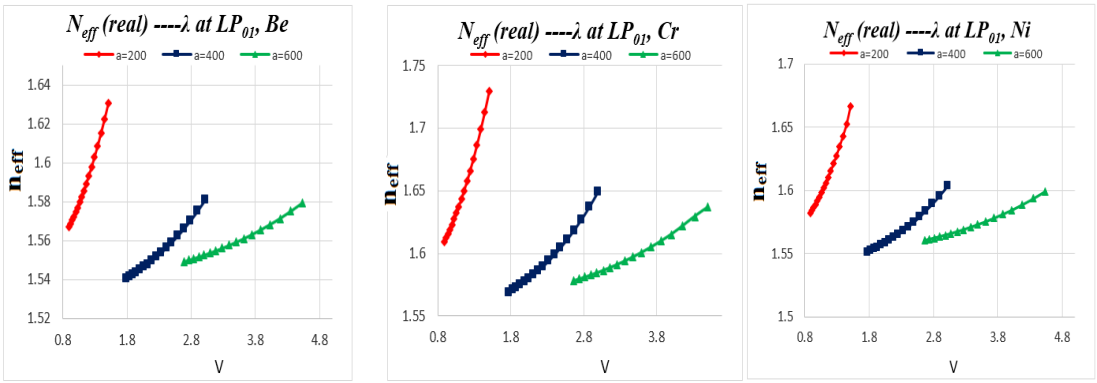

Figure 13. The dispersion relation for LP_{01} mode of the fiber cores made with *Be, Cr* and *Ni* at *a* = 200, 400, and 600 nm

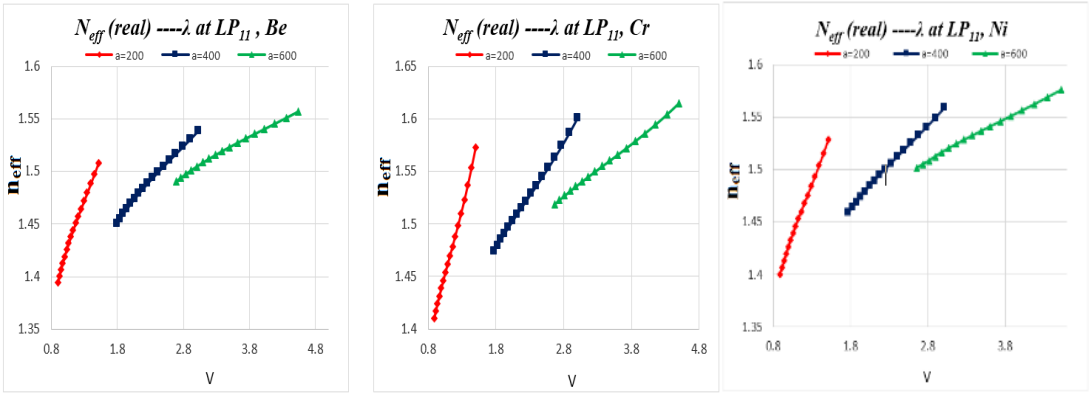

Figure 14. The dispersion relation for LP_{11} mode of the fiber cores made with *Be, Cr* and *Ni* at *a* = 200, 400, and 600 nm

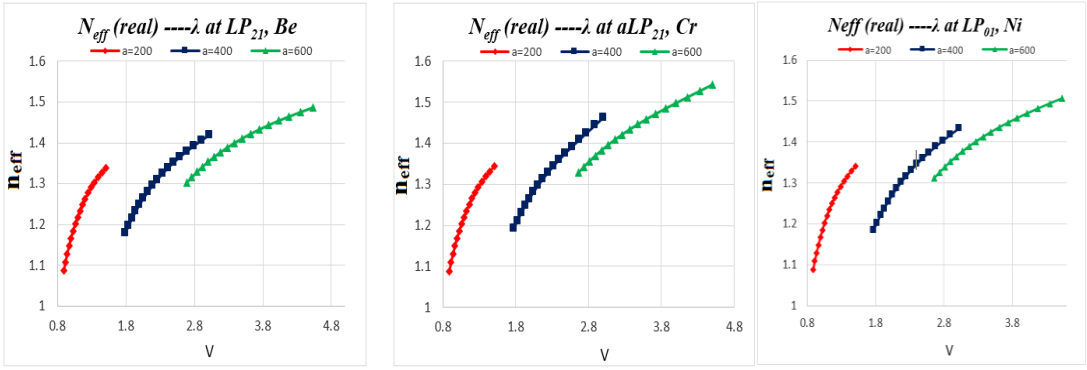

Figure 15. The dispersion relation for LP_{21} mode of the fiber cores made with *Be, Cr* and *Ni* at *a* = 200, 400, and 600 nm

A comparison of our results with other state-of-the-art research reported in the literature [31,32] suggested that the V values were highest for the core made from Be with *a* being odd. It was inferred that the highest results of the dispersion relation of the core made from different plasmonic metals followed the order of *Cr* > *Ni* > *Be* > *Au* > *Ag* > *Cu* > *Al* [32, 33].

Conclusions

The characteristics of optical fiber with plasmonic metal cores were determined for the first time. It was demonstrated that the performance of the fiber can be improved by customizing the nature of metal core, core radius and wavelength. The impact of metals cores like Be, Cr, and Ni on the modification of refractive index, dispersion relation of three modes (LP_{01}, LP_{11} and LP_{21}), attenuation coefficient, propagation constant, sensitivity and bandwidth were evaluated . COMSOL MULTIPHYSICS software with FEM was used for the calculation. It was established that thee power ratio can be balanced by increasing the fiber core radius and the wavelength of light. The values of effective refractive index, attenuation coefficient, and propagation constant were higher at shorter wavelengths. A direct correlation between effective refractive index and standard frequency was ascertained. In terms of optimum performance of the metal core it followed the trend of Cr > Ni > Be, indicating high values of *V* for Be. The LP_{01} mode appeared at a narrow range of *V* and LP_{11} and LP_{21} occurred at wider range of *V*. Briefly, the proposed fiber design can be potential for several functional devices applications.

Conflicts of Interest

The author(s) declare(s) that there is no conflict of interest regarding the publication of this paper.

Acknowledgment

This work is part of a research project UTM Fundamental Research Q.J130000.3809.22H43, supported by the Universiti Teknologi Malaysia.

References

[1] Case, K. M. (1959). Plasma oscillations. *Annals of physics*, *7*(3), 349-364.
[2] Salim, A. A., Bakhtiar, H., Shamsudin, M. S., Aziz, M. S., Johari, A. R., & Ghoshal, S. K. (2022). Performance evaluation of rose bengal dye-decorated plasmonic gold nanoparticles-coated fiber-optic humidity sensor: A mechanism for improved sensing. *Sensors and Actuators A: Physical*, *347*, 113943.
[3] Polavarapu, L., Pérez-Juste, J., Xu, Q. H., & Liz-Marzán, L. M. (2014). Optical sensing of biological, chemical and ionic species through aggregation of plasmonic nanoparticles. *Journal of Materials Chemistry C*, *2*(36), 7460-7476.
[4] Salim, A. A., Bakhtiar, H., Krishnan, G., & Ghoshal, S. K. (2021). Nanosecond pulse laser-induced fabrication of gold and silver-integrated cinnamon shell structure: Tunable fluorescence dynamics and morphology. *Optics & Laser Technology*, *138*, 106834.
[5] Zayats, A. V., Smolyaninov, I. I., & Maradudin, A. A. (2005). Nano-optics of surface plasmon polaritons. *Physics reports*, *408*(3-4), 131-314.
[6] Salim, A. A., Ghoshal, S. K., Suan, L. P., Bidin, N., Hamzah, K., Duralim, M., & Bakhtiar, H. (2018). Liquid

media regulated growth of cinnamon nanoparticles: *Absorption and emission traits. Malaysian Journal of Fundamental and Applied Sciences*, *14*(3-1), 447-449.
[7] Bertolotti, M., Sibilia, C., & Guzman, A. M. (2017). *Evanescent waves in optics: An introduction to plasmonics* (Vol. 206). Cham: Springer.
[8] Zeng, S., Yong, K. T., Roy, I., Dinh, X. Q., Yu, X., & Luan, F. (2011). A review on functionalized gold nanoparticles for biosensing applications. *Plasmonics*, *6*(3), 491-506.
[9] McEuen, P., & Kittel, C. (2005). *Introduction to solid state physics.* Eight Edition. John Wiley & Sons, Inc.
[10] Salim, A. A., Ghoshal, S. K., & Bakhtiar, H. (2021). Growth mechanism and optical characteristics of Nd: YAG laser ablated amorphous cinnamon nanoparticles produced in ethanol: Influence of accumulative pulse irradiation time variation. *Photonics and Nanostructures-Fundamentals and Applications*, *43*, 100889.
[11] Li, M., Cushing, S. K., & Wu, N. (2015). Plasmon-enhanced optical sensors: A review. *Analyst*, *140*(2), 386-406.
[12] Hämäläinen, J., Ritala, M., & Leskelä, M. (2014). Atomic layer deposition of noble metals and their oxides. *Chemistry of Materials*, *26*(1), 786-801.
[13] Capek, I. (2015). *DNA engineered noble metal nanoparticles: Fundamentals and state-of-the-art of nanobiotechnology*. John Wiley & Sons.
[14] Haque, E., Hossain, M. A., Ahmed, F., & Namihira, Y. (2018). Surface plasmon resonance sensor based on modified $ D $-shaped photonic crystal fiber for wider range of refractive index detection. *IEEE Sensors Journal*, *18*(20), 8287-8293.
[15] Erdmanis, M., Viegas, D., Hautakorpi, M., Novotny, S., Santos, J. L., & Ludvigsen, H. (2011). Comprehensive numerical analysis of a surface-plasmon-resonance sensor based on an H-shaped optical fiber. *Optics Express*, *19*(15), 13980-13988.
[16] Tuan Guo, Álvaro González-Vila, Médéric Loyez, Christophe Caucheteur. (2017). Plasmonic optical fiber-grating immunosensing: A Review. *Sensors*, *17*, 2732.
[17] Jorgenson, R. C., & Yee, S. S. (1993). A fiber-optic chemical sensor based on surface plasmon resonance. *Sensors and Actuators B: Chemical*, *12*(3), 213-220.
[18] Taylor, H. (1984). Bending effects in optical fibers. *Journal of Lightwave Technology*, *2*(5), 617-628.
[19] Gupta, B. D., Dodeja, H., & Tomar, A. K. (1996). Fibre-optic evanescent field absorption sensor based on a U-shaped probe. *Optical and Quantum Electronics*, *28*, 1629-1639.
[20] Salman, M. H., Muhammad, H. K., & Yasser, H. A. (2020). Effects of holes radius on plasmonic photonic crystal fiber sensor with internal gold layer. *Periodicals of Engineering and Natural Sciences*, *8*(3), 1288-1296.
[21] Chen, N., Chang, M., Zhang, X., Zhou, J., Lu, X., & Zhuang, S. (2019). Highly sensitive plasmonic sensor based on a dual-side polished photonic crystal fiber for component content sensing applications. *Nanomaterials*, *9*(11), 1587.
[22] Hussein Taqi John, Imad Kamil Zayer, & Ali Abed Jaber. (2023). The effect of nickel on the sensitivity of plasmonic photonic crystal fiber sensor. *Eurasian Journal of Physics,Chemistry and Mathematics*, *14*, 28-42.
[23] Paul, A. K., Sarkar, A. K., Rahman, A. B. S., & Khaleque, A. (2018). Twin core photonic crystal fiber plasmonic refractive index sensor. *IEEE Sensors Journal*, *18*(14), 5761-5769.
[24] Zeng, S., Yong, K. T., Roy, I., Dinh, X. Q., Yu, X., & Luan, F. (2011). A review on functionalized gold nanoparticles for biosensing applications. *Plasmonics*, *6*, 491-506.
[25] Al Mahfuz, M., Mollah, M. A., Momota, M. R., Paul, A. K., Masud, A., Akter, S., & Hasan, M. R. (2019). Highly sensitive photonic crystal fiber plasmonic biosensor: Design and analysis. *Optical Materials*, *90*, 315-321.
[26] Das, S., & Singh, V. K. (2020). Refractive index sensor based on selectively liquid infiltrated birefringent photonic crystal fiber. *Optik*, *201*, 163489.
[27] Arumugam, M. (2001). Optical fiber communication—an overview. *Pramana*, *57*(5), 849-869.
[28] Muhammad, H. K., Salman, M. H., & Yasser, H. A. (2020). New plasmonic photonic crystal fiber sensor based on core size. *NeuroQuantology*, *18*(9), 45.
[29] Agrawal, G. P. (2000). Nonlinear fiber optics. In *Nonlinear Science at the Dawn of the 21st Century* (pp. 195-211). Berlin, Heidelberg: Springer Berlin Heidelberg.
[30] Yang, X., Lu, Y., Liu, B., & Yao, J. (2017). Analysis of graphene-based photonic crystal fiber sensor using birefringence and surface plasmon resonance. *Plasmonics*, *12*(2), 489-496.
[31] Hu, D. J. J., & Ho, H. P. (2017). Recent advances in plasmonic photonic crystal fibers: Design, fabrication and applications. *Advances in Optics and Photonics*, *9*(2), 257-314.
[32] Salim, A. A., Ghoshal, S. K., Shamsudin, M. S., Rosli, M. I., Aziz, M. S., Harun, S. W., ... & Bakhtiar, H. (2021). Absorption, fluorescence and sensing quality of Rose Bengal dye-encapsulated cinnamon nanoparticles. *Sensors and Actuators A: Physical*, *332*, 113055.
[33] John, H. T. (2021, December). Influence metal berylliumof the optical fibercoreon plasmonic properties. *Journal of Physics: Conference Series* (Vol. 2114, No. 1, p. 012008). IOP Publishing.